Fire Safety Journal

Parametric study on axially loaded square hollow section T-joints at elevated temperatures

--Manuscript Draft--

Manuscript Number:	FISJ_2020_605R1
Article Type:	Research Paper
Keywords:	Numerical study; component method.; joint resistance; T-joint; hollow section
Corresponding Author:	Jolanta Baczkiewicz Tampere Univeristy Tampere, Finland
First Author:	Jolanta Baczkiewicz
Order of Authors:	Jolanta Baczkiewicz
	Mikko Malaska
	Sami Pajunen
	Markku Heinisuo
Abstract:	The paper presents the numerical study of tubular square T-joints under fire conditions. The sequentially coupled thermal-displacement numerical model was proposed to examine the performance of square hollow section (SHS) joints. The developed finite element (FE) model was validated against available experimental test results and applied to study the influence of dimensionless parameters on the strength of SHS tubular T-joints at elevated temperatures. These parameters include brace-to-chord width ratio β, chord-width-to-thickness ratio γ, chord-to-brace thickness ratio τ and loading ratio nF. The obtained results show that the critical temperature of T-joints is mostly influenced by the loading ratio nF and β parameter. Different methods to obtain the joint resistance are presented. The strength of the joint obtained based on EN 1993-1-8 was compared with FE analysis, which showed that the decrease in the joint resistance in brace axial compression follows the curve of Young's modulus reduction factors. Finally, the strength of the joint was calculated based on the component method, with a temperature increase specified for each individual component. This method gave higher results in joint strength, when the non-uniform temperature distribution within the joint was taken into account.
Suggested Reviewers:	František Wald frantisek.wald@cvut.cz
	Kang Hai Tan ckhtan@ntu.edu.sg
	Yongbo Shao cybshao@ytu.edu.cn
Response to Reviewers:	

Parametric study on axially loaded square hollow section T-joints at elevated temperature

Jolanta Bączkiewicz, Mikko Malaska, Sami Pajunen, Markku Heinisuo

Tampere University, Civil Engineering, Finland
jolanta.baczkiewicz@tuni.fi, mikko.malaska@tuni.fi, sami.pajunen@tuni.fi, markku.heinisuo@tuni.fi

Abstract:
The paper presents the numerical study of tubular square T-joints under fire conditions. The sequentially coupled thermal-displacement numerical model was proposed to examine the performance of square hollow section (SHS) joints. The developed finite element (FE) model was validated against available experimental test results and applied to study the influence of dimensionless parameters on the strength of SHS tubular T-joints at elevated temperatures. These parameters include brace-to-chord width ratio β, chord-width-to-thickness ratio γ, chord-to-brace thickness ratio τ and loading ratio n_F. The obtained results show that the critical temperature of T-joints is mostly influenced by the loading ratio n_F and β parameter. Different methods to obtain the joint resistance are presented. The strength of the joint obtained based on EN 1993-1-8 was compared with FE analysis, which showed that the decrease in the joint resistance in brace axial compression follows the curve of Young's modulus reduction factors. Finally, the strength of the joint was calculated based on the component method, with a temperature increase specified for each individual component. This method gave higher results in joint strength, when the non-uniform temperature distribution within the joint was taken into account.

Keywords: Hollow section; T-joint; joint resistance; numerical study; component method.

1. Introduction

The behaviour of welded tubular joints has been studied extensively at ambient temperature and design methods are available in such standards and guidelines as Eurocode EN 1993-1-8 [1] and CIDECT [2]. However, there is only limited research available on joint performance at elevated temperatures and there is a lack of fire design approaches and methods applicable for the tubular steel truss and joint design.
In fire conditions, the structural analysis and design of tubular steel trusses typically includes two resistance checks: truss members and joints between the members. In experimental and numerical studies [3,4] failure modes, temperature distribution and the effects of different geometrical parameters and load levels on the critical temperatures of steel planar CHS tubular trusses were investigated. The two trusses tested under constant loading and transient heating conditions failed, due to local buckling of the diagonal brace members. In the transient condition, the structure was first loaded up to a predefined level and then exposed to fire temperatures. Numerical simulations also demonstrated that the critical temperature of the truss can be improved significantly by increasing both the brace diameter and the wall thickness of the chord.
In their experimental and numerical research on CHS T-joints, Chen et al. [5] found that, in transient heating conditions, the joint fails, due to local plastification of the chord face around the brace-chord intersection, and the joint fails suddenly, after temperature exceeds a certain value. The experimental program included three joint specimens tested in transient conditions. The numerical study showed that the brace load level and the brace-to-chord width ratio β have a significant effect on the fire resistance of the joint. Tan et al. [6] experimentally and numerically investigated the failure mechanism and ultimate strength of CHS T-joints. Five

full-scale tests carried out in steady state conditions demonstrated that, at elevated temperatures, the plastification of the chord, local buckling and ovalisation of the joint are more concentrated around the brace-to-chord intersection. In the steady state conditions, the joints were first heated to a specific temperature and then loaded at the constant temperature. They also used the CIDECT [2] design guide to determine whether the formula of a common design code for ambient temperature conditions could be modified for elevated temperature conditions. The results were non-conservative, even if the reduction factors of steel yield strength were applied to joint resistance calculation. He et al. [7] made similar observations in their experimental research on CHS gap K-joints in transient test conditions. They also found that, in K-joints, the temperature distribution is not uniform, as the brace temperatures were higher than the chord temperatures.

Ozyurt et al. [8] carried out an extensive numerical study on different CHS and SHS joint configurations, including T-, Y-, X-, N- and K-joints under brace axial compression and tension. The simulations were carried out in steady state conditions. Numerical simulation results were compared with the calculation results produced using the design equations of Eurocode EN 1993-1-8 [1] and the CIDECT [2] design guide, by replacing the yield stress of steel at ambient temperature by material properties at elevated temperatures, in accordance with EN 1993-1-2 [9]. These simulations included SHS T-joints in brace axial compression and with the β parameter varying from 0.4 to 0.67. The results indicated that, for CHS T-joints with brace member under axial tensile load, the design equations for ambient conditions can be used, if the yield strength of steel at an ambient temperature is replaced by the strength at an elevated temperature. For CHS and SHS T-joints under brace compression load, this approach overestimates the ultimate load-carrying capacity of the joint and the simulated joint strength reduction more closely followed the reduction in the elastic modulus of steel at an elevated temperature. Ozyurt et al. [8] introduced two factors contributing to this higher reduction in joint resistance. The chord top flange is in axial compression, due to global bending of the chord member. When the brace member in compression presses the chord face down locally, this local deformation creates eccentricity for the axial compression, which in turn produces some additional bending moment in the tube wall. At the same time, the side faces of the chord member experience local bulging under the brace compression. These deformations and effects increase at elevated temperatures, as the stiffness of the steel is decreasing and the joint failure load decreases faster than the yield strength of steel at elevated temperature. Based on their results, Ozyurt et al. [8] also stated that the strength reductions at elevated temperatures are greater for CHS T-joints than for SHS T-joints, because the extent of flattening and ovalisation is much greater in the CHS section than in SHS section. As the joint strength reduction is caused by deformation of the chord member, the research proposed that the joint strength under brace compression should be related to the deformation characteristics of the joint, i.e. the reduction factor of the elastic modulus should be used, rather than the reduction of the yield strength.

The resistance of stainless-steel SHS, RHS and CHS tubular X- and T-joints subjected to brace axial compression at elevated temperatures was numerically investigated by Lan and Huang [10]. The steady state analysis was performed for a wide range of geometric parameters. For SHS T-joints the β parameter values studied were 0.2, 0.4 and 1. The same analogy as in the study presented by Ozyurt et al. [8] was utilized to obtain the resistance of stainless-steel joints at elevated temperature. The reduction of the joint strength was compared with the reduction factors of yield strength and elastic modulus of stainless-steel. The results showed that for tubular stainless-steel T- and X-joints under brace axial compression load the average value of the steel yield strength and elastic modulus reductions can be used as the joint strength reduction factor at an elevated temperature.

He et al. [11] introduced the joint design method based on critical temperature and a failure criteria for CHS K-joints. The joint is considered to be safe when the joint temperature is lower than a critical temperature. It was demonstrated that the conventional $3\%b_0$ deformation limit is not a suitable criterion for fire conditions where the deforming rate is very fast, and joints may collapse in a very short time. A limit for the deforming rate was proposed and the critical state was defined as k = 0.1 mm/°C, which means that the critical temperature is reached when the joint displacement increases by 1 mm, as the steel temperature increases by 10 °C. The equation of EN 1993-1-2 [9] used for calculating the temperature development of a steel member was found suitable and sufficiently conservative to predict the temperature development of a CHS K-joint for design purposes. Also, the equation of EN 1993-1-2 [9] to predict the critical temperature of a steel member was proposed for critical temperature calculations of CHS K-joints.

Shao et al. [12] experimentally studied the effects of initial chord stress on the resistance of CHS T-joints in transient heating conditions. In their study, the brace-to-chord ratios β of the specimens were 0.37 and 0.61, respectively. The uniform axial initial chord stress levels applied to the chord members were 0 – 30 % of the yield load of the chord sections at ambient temperature. The axial compression loads applied at the brace end were 50 % of the joint resistance determined through finite element analysis. The failure mode of all the tested specimens was characterized by chord plastification around the brace-chord intersection. The research concluded that, by using the reduction factors of the elastic modulus to modify the yield stress in the equations of EN 1993-1-8 [1], CIDECT [2] and API RP 2A WSD [13], it was possible to calculate a safe prediction of the static design axial resistance of welded CHS T-joints at elevated temperatures.

Shao et al. [14] studied the static strength of CHS K-joints at elevated temperatures and proposed a design method and equations to predict the static axial resistance of K-joints at elevated temperatures. The resistance can be determined by combining the revised reduction factor of elastic modulus, a revised chord stress ratio and the static axial resistance of a welded K-joint at ambient temperature. Shao et al. [14] also highlighted that transient state has been considered more appropriate and practical for the fire engineering of joints, because in transient conditions, the specimen is in a similar situation to a structure in a real fire. The accuracy and reliability of the methods and equations, based on the assumption that the joints are in a steady state condition during heat transfer, should be verified and benchmarked through experimental results.

All of the above research was related to CHS T- and K-joints, except the numerical simulations of SHS T-joints under brace compression load reported by Ozyurt et al. [8] and for stainless steel SHS T-joints reported by Lan and Huang [10]. Experimental research on SHS joints under brace compression and in transient heating conditions has been conducted by Yang et al. [15] and Bączkiewicz et al. [16]. In the study by Yang et al. [15], two joints were tested with β parameters equal to 0.4 and 0.8, respectively. The specimens had identical brace and chord wall thicknesses. The results indicated that the brace–chord intersection area is the most likely to buckle and that the characteristics of the deforming process were depend on the joint geometry. For both specimens, the failure mode consisted of local buckling of the chord surface near the brace–chord intersection; however, buckling of the chord side walls for the specimen with β parameter equal to 0.8 was also observed. The researchers did not analyse joint strength in more detail.

Bączkiewicz et al. [16] tested five SHS T-joints under brace axial compression to investigate joint temperature development, critical steel temperatures, failure process and failure modes of the specimens with different β parameter values. Three failure modes were observed, and the test results indicated that joint geometry affects the failure mode. Steel temperature distributions measured during the tests were not uniform and the non-uniformity may affect

the joint resistance at elevated temperatures. Based on the test results, joint geometry is a determining factor of the joint failure type. For joints with small values for the β parameter, the failure mode at elevated temperatures consisted of plastic failure on the chord face at the brace–chord intersection. For specimens with a β parameter of $0.85< \beta <1$, the failure consisted of buckling of the chord side wall. However, due to high temperatures, the plastification of the top wall of the chord also occurred. For a joint with a β parameter of $0.85< \beta <1$ and relatively thin chord walls, the failure mode consisted of a combination of buckling of the chord side wall and plastic yielding of the brace side wall. The failure modes observed were the same as the failure modes for the respective joints at ambient conditions, calculated according to EN 1993-1-8 [1]. At high temperatures, the plastification of the side and top walls of the chord is more significant than it is at normal temperatures.
The above review shows that there is no design method or equation verified in transient test conditions available to predict the static axial resistance of welded SHS T-joints at elevated temperatures. More information on the effects of different joint geometry and loading conditions is required. In this paper, a numerical study was carried out to deepen and extend knowledge of SHS T-joint behaviour under fire conditions and to create data for the method development. The numerical simulation model used in this study was calibrated and validated against the experimental results of Bączkiewicz et al. [16]. Also, a design method based on Eurocode equations was proposed to predict the failure and static axial resistance of SHS T-joints at elevated temperatures.

2. Methodology

The purpose of this study was to investigate methods to numerically obtain the axial resistance of an SHS T-joint at elevated temperatures, based on steel temperature and failure criteria. The joint performance and mechanisms of failure were first studied using a finite element (FE) model developed and validated in a previous study by the authors [16]. The analysis covered β parameter values of 0.5, 0.6 and 0.9. Observations from experimental tests and numerical simulations were used to confirm the joint failure mechanisms and modes. The main results regarding failure modes are reported in the introduction above. The summary of model validation is reported in Section 3.

A parametric study was then carried out in the temperature domain to investigate the effects of geometrical parameters and loading ratio on the joint performance and critical temperature of T-joints. Geometrical parameters included β (brace-to-chord diameter ratio), γ (ratio of the chord width to twice its wall thickness) and τ (brace-to-chord wall thickness ratio). Fire resistance of the joints was then studied in the strength domain to verify the correct level of reduction in steel yield strength. Experimental and numerical results were compared with those calculated using the equations of EN 1993-1-8 [1].

Previous research by Bączkiewicz et al. [17,18] showed that the temperature distribution within the joint area is non-uniform, which affects the fire resistance of individual connection components. The component method was used to investigate the influence of different component temperatures on the joint resistance and failure modes. The aim was to investigate whether it is safe to use one constant temperature for joint design and whether the equation of EN 1993-1-2 [9] for steel temperature development is a valid method to determine the temperature of an SHS T-joint. The above approach was aimed at developing a simple design method to evaluate the fire resistance of an SHS T-joint in fire conditions. The following sub-sections introduce the theoretical background of the study.

2.1. Fire resistance of tubular T-joints in the strength domain

In this study, the method suggested by Zhao [19], who implied a deformation limit introduced by Lu et al. [20], was used to obtain the ultimate resistance of a joint. The joint resistance is determined by comparing the joint deformation δ_{max} associated with the maximum load N_{max} during the loading history and the deformation limit of $3\%b_0$, where b_0 is the width of the chord section. If the maximum load N_{max} corresponds to a deformation smaller than $3\%b_0$, then the N_{max} is assumed to be the ultimate resistance of the joint (see Figure 1). If the maximum load corresponds to a deformation greater than $3\%b_0$, then the resistance depends on the ratio of $N_{3\%b0}$ to $N_{1\%b0}$, where $N_{3\%b0}$ and $N_{1\%b0}$ are load levels associated with joint deformations of $3\%b_0$ and $1\%b_0$, respectively. For joints with a ratio $N_{3\%b0}/ N_{1\%b0}$ lower than 1.5, the ultimate resistance is assumed to be $N_{3\%b0}$ (see Figure 2 a)), and for joints where the ratio $N_{3\%b0}/ N_{1\%b0}$ is greater than 1.5, the ultimate resistance is assumed to be $1.5N_{1\%b0}$ (see Figure 2 b)). The method is analytically represented by Equation (1). This approach does not require any curve-fitting and can therefore be applied to all SHS T-joints, including chord face plastification and side wall buckling failure modes.

$$N_{ult} = \begin{cases} N_{max}, & \delta_{max} \leq 3\%b_0 \\ N_{3\%b_0}, & \delta_{max} > 3\%b_0 \ \cup \ \frac{N_{3\%b_0}}{N_{1\%b_0}} < 1.5 \\ 1.5N_{1\%b_0}, & \delta_{max} > 3\%b_0 \ \cup \ \frac{N_{3\%b_0}}{N_{1\%b_0}} > 1.5 \end{cases} \quad (1)$$

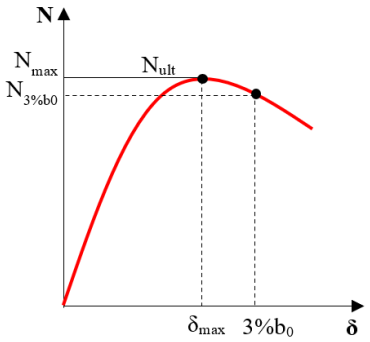

Fig. 1. Ultimate resistance of tubular T-joints for $\delta_{max} \leq 3\%\ b_0$, where δ_{max} is the joint deformation associated with the maximum load N_{max} during the loading history [19].

a)

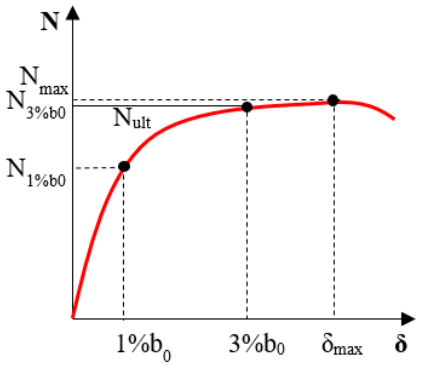

b)

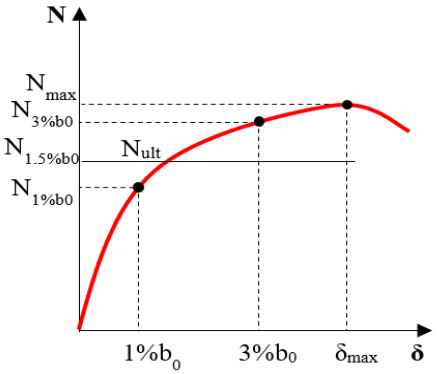

Fig. 2. Ultimate resistance of tubular T-joints for $\delta_{max} > 3\%\ b_0$; a) $N_{3\%b0}/N_{1\%b0}<1.5$, b) $N_{3\%b0}/N_{1\%b0}>1.5$ [19].

At ambient temperature, the above presented principles are used in design codes worldwide. This study investigated the joint design from the Eurocode perspective and resistance calculations were based on standard EN 1993-1-8 [1]. The axial resistance of an SHS T-joint was calculated using the equations presented in Figure 3.

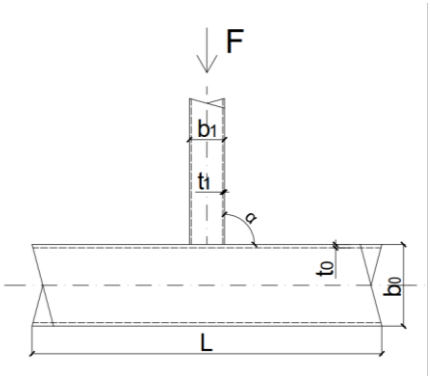

- Chord face failure, $\beta \leq 0.85$

$$N_{1,Rd} = \frac{k_n f_{y0} {t_0}^2}{(1-\beta)}\left(2\eta + 4\sqrt{1-\beta}\right)/\gamma_{M5}$$

η is equal to β for SHS-section.

- Chord side wall buckling, $\beta = 1.0$

$$N_{1,Rd} = k_n f_b t_0 (2h_1 + 10t_0)/\gamma_{M5};$$

- Brace failure, $\beta \geq 0.85$

$$N_{1,Rd} = f_{yi} t_1 (2h_1 - 4t_1 + 2b_{eff})/\gamma_{M5}$$

- Punching shear, $0.85 \leq \beta \leq (1\text{-}1/\gamma)$

$$N_{1,Rd} = \frac{f_{y0} t_0}{\sqrt{3}}\left(2h_1 + 2b_{e,p}\right)/\gamma_{M5}$$

$$f_b = \chi f_{y0}$$

$$k_n = 1{,}3 - \frac{0{,}4n}{\beta}; \quad n = \frac{\sigma_{0,Ed}}{f_{y0}}/\gamma_{M5}$$

The reduction factor for flexural buckling χ was obtained from EN 1993-1-1 [21], using the relevant buckling curve and a normalized slenderness for SHS joints given in EN 1993-1-8 [1].

$$\sigma_{0,Ed} = \frac{N_{0,Ed}}{A_0} + \frac{M_{0,Ed}}{W_{el,0}}$$

Fig. 3. Design axial resistance of welded SHS T-joints in compression [1].

Currently, there is no design method to calculate the resistance of lattice girders and their joints at elevated temperatures. However, it may be possible to adopt the equations for ambient temperature design from EN 1993-1-8 [1], by replacing the yield strength of steel at ambient temperature with corresponding strength values at elevated temperatures. The equations for ambient temperature were derived assuming small deflection at the chord face, and, their suitability for fire design conditions therefore needed to be checked.

2.2. Application of the component method to SHS T-joints

Another approach to determine the axial resistance of tubular joints is the component method, which was developed to characterize the mechanical properties of structural joints. The method was first developed for open section joints, but it has now been extended to cover tubular joints. The principles and analogies of the method used for tubular joints were developed in two CIDECT projects, 5BP (Jaspart et al. [22]) and 16F (Weynand et al. [23]). Technical specification (TS) documents [24, 25] complement Chapter 7 of standard EN 1993-1-8 [1] and provide an alternative to the semi-empirical joint resistance design formulae.

In general, the component method can be described as a three-step procedure: first, the constitutive individual components of the joint are identified; second, the stiffness and resistance properties of all of these components are determined; and finally, the single components are combined to derive the stiffness and resistance properties of the whole joint.

The method assumes the load is transferred from the brace to the chord through four loading zones located in the corners of the brace, as shown in Figure 4a. This has been justified by observations showing that elastic stresses along the cross-section of the brace are non-uniform and that the stresses concentrate in the corners of the section [26]. The four loading zones are then replaced by a system of linear springs, as illustrated in Figure 4b. Each individual spring represents a component of a welded SHS connection and has its own resistance $F_{i,Rd}$ and stiffness [23, 27]:

a. chord face in bending,
b. chord side walls in tension or compression,
c. chord side walls in shear,
d. chord face under punching shear,
e. brace flange/webs in tension/compression,
f. chord section in distortion and
g. welds.

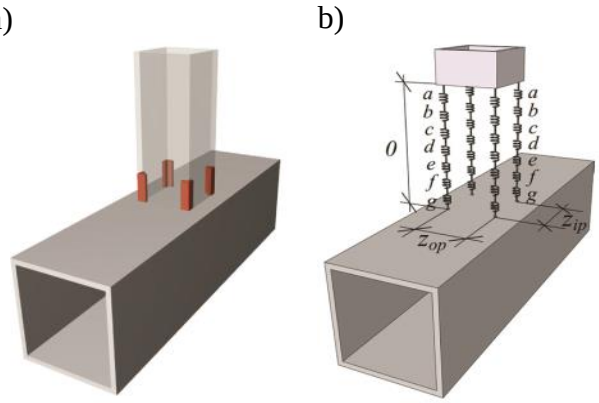

Fig. 4. Component method calculation model for SHS T-joint: a) loading zones at brace corners highlighted in brown; b) component model composed of a system of linear springs [27].

Based on experimental results, four of the above connection components must be considered in the case of an SHS T-joint in axial brace compression. These are a, b, d and e. The resistance properties of these components can be determined using the equations below. All of the additional parameters required to calculate the resistance of the components can be found in [22].

a. chord face in bending $F_{a,Rd} = \left(0{,}5l_{eff,1,a} + l_{eff,2,a}\right)k_{N,chord,a}m_{pl,Rd}$
b. chord side walls in tension or compression
$$F_{b,Rd} = k_{N,chord,b}k_{b,chord}\chi b_{eff,b}f_{y0}t_0/\gamma_{M5} \quad (2)$$
d. chord face under punching shear $F_{d,Rd} = \frac{b_{eff,d}f_{y0}t_0}{\sqrt{3}}/\gamma_{M5}$
e. brace flange/webs in tension/compression $F_{e,Rd} = b_{eff,e}f_{yi}t_1/\gamma_{M5}$

In this research, the component method was applied to fire design of the SHS joints. The aim of the study was to determine the difference in joint resistance values, calculated assuming non-uniform and uniform joint temperature distributions. Following the analogy presented by Ozyurt [8], the joint resistances were first determined assuming a non-uniform temperature distribution and calculating the resistance of each connection component separately. The resistances were determined using strength reduction factors based on the actual temperature

in each connection component. The equations (2) developed by Jaspart et al. [22] were modified by adding a coefficient of strength reduction to obtain the resistance of the joint component at a given temperature. The formulas for the temperature dependent resistance values of each component are presented in Equation (3). For the uniform temperature solution, the steel joint temperature was calculated according to EN 1993-1-2 [9]. The resistance properties of the connection components at elevated temperatures $F_{i,Rd,fi}$ were then calculated using the yield strength reduction factors $k_{y,i,\theta}$ of EN 1992-1-3 (i = a, b, d and e).

$$\begin{aligned} F_{a,Rd,fi} &= F_{a,Rd}k_{y,a,\theta} \\ F_{b,Rd,fi} &= F_{b,Rd}k_{y,b,\theta} \\ F_{d,Rd,fi} &= F_{d,Rd}k_{y,d,\theta} \\ F_{e,Rd,fi} &= F_{e,Rd}k_{y,e,\theta} \end{aligned} \quad (3)$$

The resistance of a loading zone corresponds to the minimum resistance value of the four connection components. The resistance of a T-joint consisting of four equally loaded loading zones can then be calculated from:

$$N_{1,Rd} = 4\left[F_{min,Rd,fi}\right]_1 \quad (4)$$

3. Numerical model of SHS T-joints at elevated temperatures

The finite element model introduced in Bączkiewicz et al. [16] was used in this numerical study. The model was created in Abaqus CAE software version 2017 [28] and validated against experimental fire test results reported in [16]. The model implementation represented the actual joint behaviour well and the accuracy of results was good for the SHS T-joints and loading conditions studied. Experimental tests included five joint specimens with different steel section sizes, brace loading and chord stress levels.

For the numerical simulations and parametric study reported in this paper, the implementation of thermal and stress analysis models, element types and boundary conditions are the same as presented in [16]. The geometry and mechanical boundary conditions of a typical SHS T-joint specimen of [16] are illustrated in Figure 5. The ends of the chord were considered fixed, while the brace was free to move in the direction of the brace longitudinal axis. The length of the chord and brace members were 1250 mm and 800 mm, respectively. The geometric dimensions of the specimens and axial brace compression loads applied in the tests are reported in Table 1. Also reported are the critical temperatures and failure modes obtained from the test results.

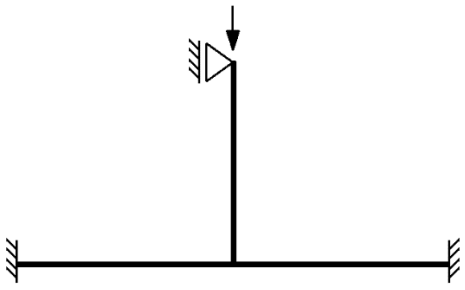

Fig. 5. Mechanical boundary conditions.

The sequentially coupled thermal-stress analysis with 20-nodes of quadratic solid brick element was adopted. For the thermal analysis, DC3D20 elements were used, and for the stress analysis, C3D20R elements with reduced integration were used. The geometry of the joints and the method of mesh generation were the same for both types of analysis. A typical finite element model is shown in Figure 6. There is no direct contact modelled between the chord and brace

members. Forces are transferred through welds, which are connected to brace and chord members with tie constraints, marked as red lines in Figure 6 c). The temperature fields obtained from the heat transfer analysis were applied as a field variable in the stress analysis. The combination of the two analyses gave the stress and deformation progression in correspondence with the temperature development. The steel material properties used in this research were from tensile tests conducted at ambient temperature by Bączkiewicz et al. [16]. The material reduction factors of EN 1993-1-2 [9] were applied at elevated temperatures.

The numerical model was validated against the experimental tests results reported in [16]. Figure 7 presents the comparison of the local vertical joint displacement versus temperature curves obtained in the experimental test and numerical analysis of specimen L4. It can be seen that the model implementation represents the actual joint behaviour well and the accuracy of results was good for the SHS T-joints and loading conditions studied. In [16] the verification of the model was carried out to find the most suitable mesh pattern for the analysis. In the sensitivity study, 8-nodes linear brick elements C3D8 and quadratic brick elements C3D20R were analysed for different mesh sizes. The study showed that the C3D20R elements with a dense mesh give best representation of the tests results, as illustrated in Figure 8.

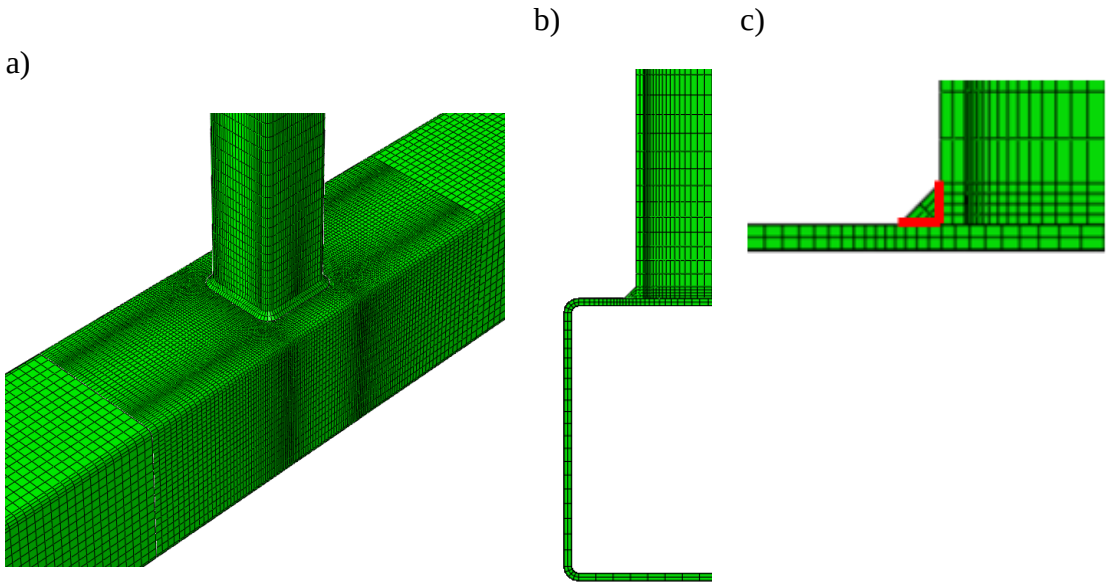

Fig. 6. Finite element model of the tubular T-joint: a) overall view; b) cut through cross-section; c) tie constrain between weld and SHS sections.

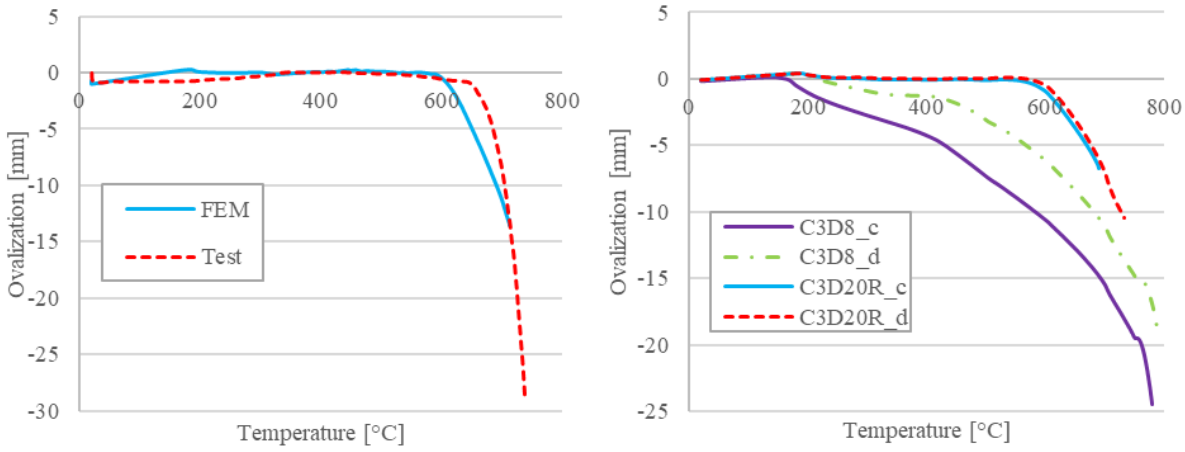

Fig. 8. Mesh sensitivity study results [16].

Fig. 7. Validation of the FE model by comparing the simulated local vertical joint displacement versus temperature curve with the experimental test result of specimen L4 [16].

Tab. 1. Details of SHS T-joint specimens and critical joint temperatures [16].

Specimen	Chord		Brace		β	Applied brace load F	Critical temperature	Failure mode
	b_0	t_0	b_1	t_1	[-]	[kN]	[°C]	
L1	200	5	100	5	0.5	24	677	Chord face failure
L2	200	5	180	5	0.9	83	682	Chord side wall buckling
L3	200	8	180	5	0.9	234	650	Chord side and brace wall buckling
L4	200	5	120	5	0.6	29	667	Chord face failure
L5	200	5	180	5	0.9	83	686	Chord side wall buckling

In the following, the experimental data of [16] and FE analysis are applied to investigate the plastification of the joints and sections. In Figure 9, the joint deformations observed in the experimental tests are compared with numerical simulation results in which the respective furnace temperature is applied to simulate fire conditions. The simulated deformations and stresses, shown at critical temperatures, are presented in Table 1.

Joint specimens L1 and L4 had brace members significantly smaller than the chord sections, parameter β being 0.5 and 0.6 for L1 and L4, respectively. The deformation of the joints proceeded gradually. In the first phase, the stress levels increased in the chord top wall along the face of the brace member, with stress concentration in the brace corner areas. As the temperature increased, high stresses also occurred at the top corners of the chord cross-section. Although stresses increased over the entire joint area, the highest stresses concentrated in the chord top face around the brace-chord intersection. The joints failed, due to plastic yielding of the chord top face. The deformed shapes of joint specimens correspond well to the observations presented.

Specimens L2, L3 and L5 had brace members, which were only slightly smaller than the chord sections. For these three specimens, β parameter was equal to 0.9. Specimens L2 and L5 were identical. In the specimen L3, a chord section with thicker wall thickness was used. The stress peaks occurred first in the chord top flange in the vicinity of the chord-brace intersection. As the temperature increased, stress peaks also formed at the top half of the chord side walls. The stresses of the chord top flange and side walls increased until the failure of the joint. In specimen L3, stress peaks also occurred in the brace side walls. As the temperature rose, the stresses increased most significantly in the side walls of the chord. The stress levels in the brace and chord side walls increased until the failure of the joint. The deformed shapes of the tested specimens support the observations.

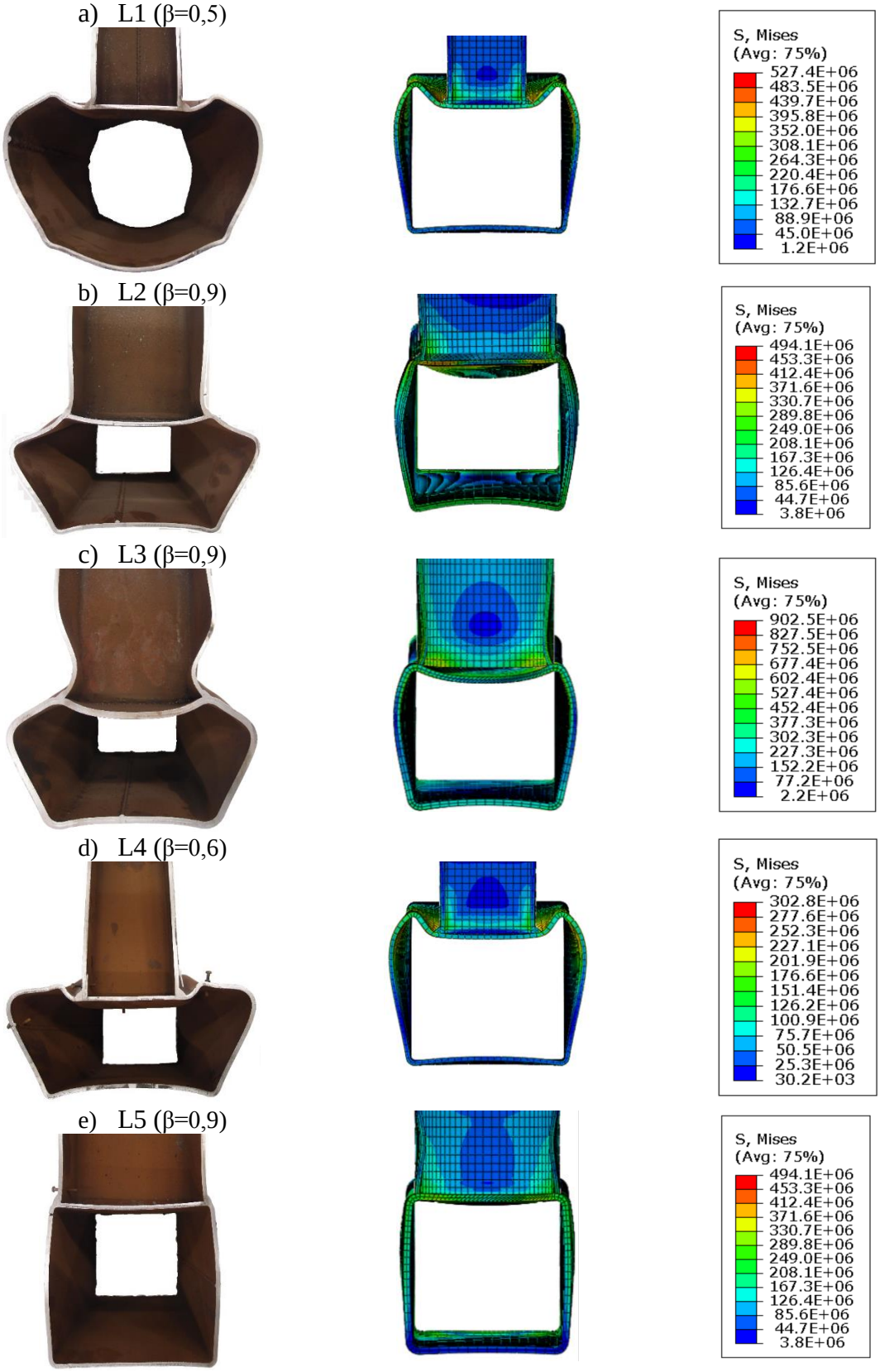

Fig. 9. Comparison of experimentally and numerically determined failure mode shapes for specimens L1-L5: a) L1; b) L2; c) L3; d) L4; e) L5.

The comparison of the FE results and the experimental data shows that the verified model simulates the joint performance with sufficient accuracy for a relatively wide range of joint β

parameters and various failure modes. Numerical analysis results confirmed the findings and observations in the experimental tests and provided more detailed information about the plastification and failure mechanisms of the joints.

4. Parametric study

A parametric study was performed to investigate the effects of different parameters on the performance of SHS T-joints at elevated temperatures focused on the effects on critical temperature. In the previous section, the numerical model, which was applied to simulate the behaviour of tubular SHS T-joint at elevated temperatures, was presented. The geometrical parameters included in the study were β, γ and τ, where β is the brace width (b_1) to chord width (b_0) ratio, γ the chord width (b_0) to double chord thickness ($2t_0$) ratio and τ the ratio of chord thickness (t_0) to brace thickness (t_1). Also, the loading ratio n_F was included in the investigation. Table 2 shows the details of the models and parameters considered in the study. Table 2 also includes the axial compression resistance of the joints at the ambient temperature N_{Rd} calculated based on EN 1993-1-8 [1]. Parameter n_F is the ratio of the load applied at the end of the brace to the axial resistance of the joint, i.e. $F = n_F N_{Rd}$. It was verified that, for the given models and loads, the initial chord stress levels caused by the bending of the chord member were low (chord stress ratio $n \leq 0.25$) and they had no influence on the resistance of the joint N_{Rd}.

In the figures below, the joint temperature refers to chord top face temperature and the joint displacement is defined as the difference between the chord top and bottom face displacements. A negative displacement means that the distance between the chord top and bottom face is decreasing. The criterion proposed by He et al. [7] was used to predict the critical temperature. The critical state was considered to have been reached when the rate of joint deformation reached a value of 0.1 mm/°C.

Tab 2. Details of T-joint models

Models	b_0 [mm]	t_0 [mm]	b_1 [mm]	t_1 [mm]	τ t_0/t_1	β b_1/b_0	γ $b_0/2t_0$	n_F [-]	N_{Rd} kN	F kN
P1	200	5	80	5	1.0	**0.4**	20	0.3	81	24
P2	200	5	100	5	1.0	**0.5**	20	0.3	95	29
P3	200	5	120	5	1.0	**0.6**	20	0.3	116	35
P4	200	5	140	5	1.0	**0.7**	20	0.3	149	45
P5	200	5	160	5	1.0	**0.8**	20	0.3	211	63
P6	200	8	180	5	1.0	**0.9**	20	0.3	315	95
P7	200	10	120	10	1.0	0.6	**10**	0.3	473	142
P8	200	8	120	8	1.0	0.6	**13**	0.3	303	91
P9	200	6	120	6	1.0	0.6	**17**	0.3	167	50
P10	200	5	120	5	1.0	0.6	**20**	0.3	116	35
P11	200	4	120	4	1.0	0.6	**25**	0.3	74	22
P12	200	5	120	5	1.0	0.6	20	**0.3**	116	35
P13	200	5	120	5	1.0	0.6	20	**0.4**	116	46
P14	200	5	120	5	1.0	0.6	20	**0.5**	116	58
P15	200	5	120	5	1.0	0.6	20	**0.6**	116	70
P16	200	5	120	5	1.0	0.6	20	**0.7**	116	81
P17	200	5	120	5	1.0	0.6	20	**0.8**	116	93
P18	200	5	120	5	1.0	0.6	20	**0.9**	116	104

P19	200	8	120	4	**2.0**	0.6	12.5	0.3	303	91
P20	200	8	120	5	**1.6**	0.6	12.5	0.3	303	91
P21	200	8	120	8	**1.0**	0.6	12.5	0.3	303	91
P22	200	6	120	8	**0.8**	0.6	16.7	0.3	167	50
P23	200	5	120	8	**0.6**	0.6	20	0.3	116	35

4.1. Effect of width ratio β

The effects of parameter *β* on the critical temperature of the SHS T-joint were analysed, using six models P1- P6. The values of *β* ranged from 0.4 to 0.9. Figure 10 shows the relationship between the joint displacement and temperature. The effect of *β* on the critical temperature is shown in Figure 11 and the critical temperatures for each analysed case are listed in Table 3. The results indicate that the critical temperature is highly dependent on *β*. The maximum temperature was achieved when *β* is 0.8. Critical temperatures were significantly lower for *β*-values less than 0.5.

Figure 10 shows that some joints (P4-P6) first experienced a positive displacement, which was caused by restrained heat expansion with fixed boundaries at the chord ends. Displacements began to increase in the negative direction when the elastic modulus and the stiffness of the chord side walls started to decrease and the walls bulged out. It appeared that, for joints that had a low value of β, there was a sudden increase in displacements at a temperature of 200 ℃. This corresponds to the temperature at which the elastic modulus of steel began to decrease.

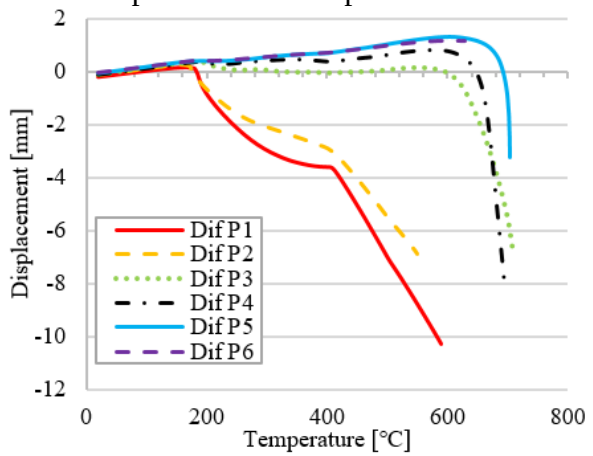

Fig. 10. Displacement-temperature curves with different values of parameter *β*.

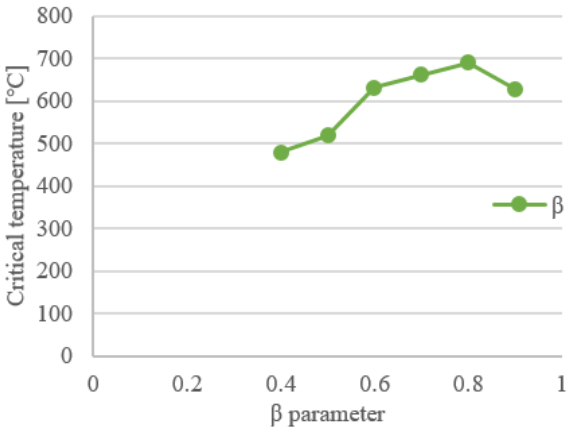

Fig. 11. Effect of parameter *β* on critical temperature of RHS T-joint.

Tab 3. Effect of *β* on critical temperature.

Model	*β*	Critical temperature [°C]
P1	0.4	479
P2	0.5	519
P3	0.6	632
P4	0.7	663
P5	0.8	691
P6	0.9	629

4.2. Effect of width/thickness ratio γ

Models P7-P11 were used to study the effects of parameter γ on the critical temperature. Values of γ included in the study were 10, 13, 17, 20 and 25. The joint displacement-temperature curves are illustrated in Figure 12 and the effects of γ on critical temperature are presented in Figure 13 and Table 4. The results show clearly that γ has only a minor effect on the critical temperature of the joint.

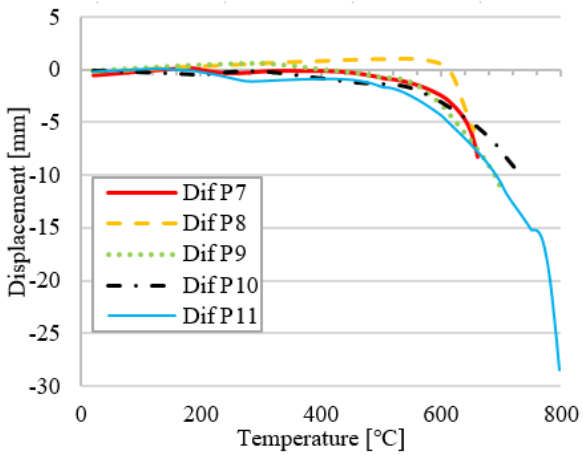

Fig. 12. Displacement-temperature curves with different values of parameter γ.

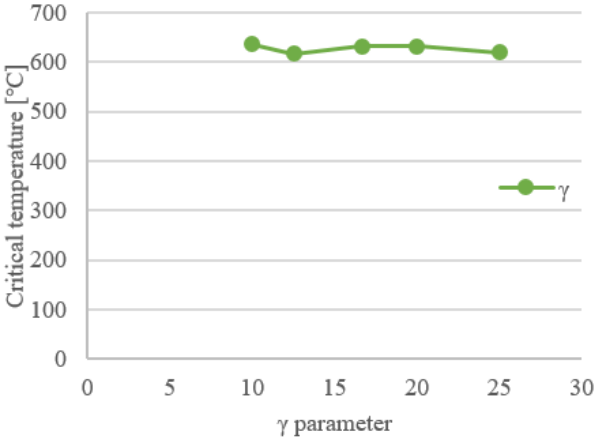

Fig. 13. Effect of parameter γ on critical temperature of T-joint.

Tab 4. Effect of γ on critical temperature and time.

Model	γ	Critical temperature [°C]
P7	10	636
P8	13	617
P9	17	632
P10	20	632
P11	25	619

4.3. Effect of chord thickness τ

The effect of chord and brace wall thicknesses was analysed using Models P19-P23. Parameter τ varied from 2.0 to 0.6. The joint displacement-temperature curves are illustrated in Figure 14 and the effects of τ on critical temperature are presented in Figure 15 and Table 5. The results indicate that τ does not affect the critical temperature. The optimum solution was achieved when the brace and chord wall thicknesses were the same.

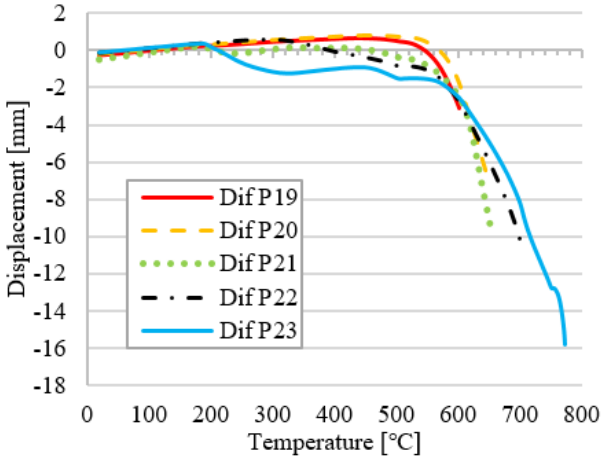

Fig. 14. Displacement-temperature curves with different values of parameter τ.

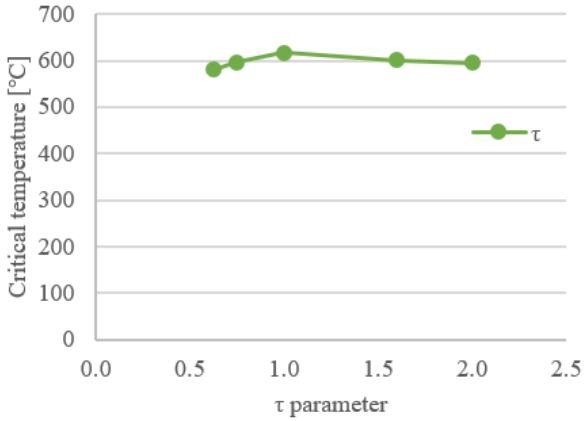

Fig. 15. Effect of parameter τ on critical temperature of T-joint.

Tab. 5. Effect of τ on critical temperature and time.

Model	τ	Critical temperature [°C]
P19	2.0	596
P20	1.6	600
P21	1.0	617
P22	0.8	597
P23	0.6	581

4.4. Effect of load ratio n_F

The effect of the loading ratio n_F on the critical temperature was studied using models P12 – P18, in which the loading ratio n_F varied from 0.3 to 0.9. The joint displacement-temperature curves are illustrated in Figure 16 and the effects of n_F on critical temperature are presented in Figure 17 and Table 6. It can be seen that the critical temperature decreased almost linearly as the brace axial load increased. Critical temperature decreased from 632 ℃ to 483 ℃ when the loading ratio was increased from 0.3 to 0.9.

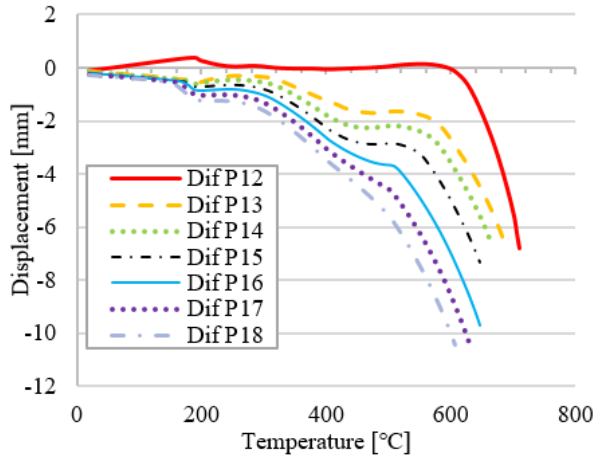

Fig. 16. Displacement-temperature curves with different values of parameter n_F.

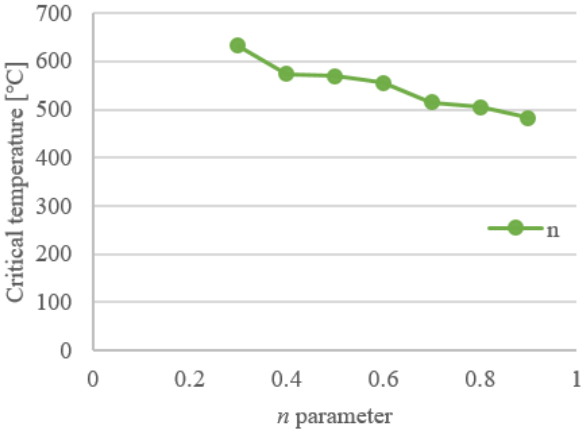

Fig. 17. Effect of parameter n_F on critical temperature of T-joint.

Tab. 6. Effect of n_F on critical temperature and time.

Model	n_F	Critical temperature [°C]
P12	0.3	632
P13	0.4	574
P14	0.5	569
P15	0.6	556
P16	0.7	514
P17	0.8	505
P18	0.9	483

Based on the results of 23 numerical simulations, the effects of geometrical parameter β and load ratio n_F do affect the critical temperature and they must be considered in the design. Parameters γ and τ have minor or no effect on critical temperature and their effects can be ignored.

5. Static axial resistance of a SHS T-joint

Previous studies introduced a design method to determine the axial resistance of welded CHS T-joints at elevated temperatures [8, 12]. The research concluded that a safe prediction of the static design axial resistance can be calculated by using the reduction factors of the elastic modulus [9] to modify the yield stress in the equations of EN 1993-1-8 [1]. Based on four numerical simulations by Ozyurt et al. [8], the method may also be applicable to SHS T-joints. In the following, the design approach is validated by experimental test results [16] and by simulating the joint performance numerically in steady state conditions.

First, the specimens from experimental tests [16] were analysed. The critical temperatures obtained in experimental tests are listed in Table 7. For each temperature, the corresponding reduction factors of steel yield strength ($k_{y,\theta}$) and elastic modulus ($k_{E,\theta}$) were calculated according to [9]. The joint axial resistances at critical temperature were then calculated by multiplying the joint resistance in ambient conditions by the reduction factors, separately for $k_{y,\theta}$ and $k_{E,\theta}$. The joint resistance at a normal temperature was calculated using equations of Figure 3 and the steel material properties reported in [16]. Table 7 shows that the joint resistance values predicted using the yield strength reduction were higher than the test loads reported in Table 1 and this reduction overestimates the joint resistance. The last column of Table 7 show that the method leads to conservative and safe resistance values when the elastic modulus reduction is applied. However, by applying the elastic modulus reduction factor, the method underestimates the joint resistance significantly, up to 70%.

Tab. 7. Joint axial resistances at experimentally determined critical temperatures and as calculated according to the formulae of EN 1993-1-8 [1] and using the reduction factors of EN 1993-1-2 [9].

Specimen	Critical temperature [°C]	$k_{y,\theta}$ [-]	$k_{E,\theta}$ [-]	Resistance at normal temperature $N_{1,Rd}$ [kN]	Resistance at critical temperature $N_{1,Rd}\ k_{y,\theta}$ [kN]	Resistance at critical temperature $N_{1,Rd}\ k_{E,\theta}$ [kN]
L1	677	0.29	0.17	95	27	16
L2	682	0.27	0.16	315	86	51
L3	650	0.35	0.22	899	315	198
L4	667	0.31	0.19	116	36	22

L5	686	0.26	0.16	315	83	49

The results of Table 7 are inconclusive and further analysis was carried out to investigate the accuracy of the method at different joint temperature levels. The joint configurations listed in Tables 1 and 2 were simulated numerically in steady state conditions. For each joint, a force-displacement curve was produced at different temperature levels by using FE analysis. The ultimate resistance of a joint at a specific temperature was then determined using the curve produced and the criteria introduced in Figures 1 and 2. Joint temperatures considered ranged from 100 ℃ up to 800 ℃. Simulated resistance values were then compared against the axial compression resistance of the joints at the ambient temperature $N_{1,Rd,}$ calculated based on EN 1993-1-8 [1] and reported in Table 7. The reduction coefficient for each joint configuration was then calculated as the ratio of ultimate resistance at temperature θ to the resistance at the ambient temperature.

Figure 18 presents the conservative estimation of force-displacement curves simulated at 500 ℃ for the test specimens of Table 1. Similar curves were simulated at all eight temperature levels and the corresponding reduction factors are presented in Table 8 and illustrated in Figure 19. Figure 19 (b) presents the average value of the reduction factors obtained for the specimens at specific temperature level, compared to the yield strength, elastic modulus reductions provided by EN 1993-1-2 [9] and mean value of the yield strength and elastic modulus reduction factors. The results demonstrate that the decrease in joint resistance followed the elastic modulus reduction very well, and the calculated results are conservative estimations of the joint resistance. Steel yield strength reduction and the mean value of the yield strength and elastic modulus reduction factors tended to overestimate the resistance. Simulations carried out for the joint models listed in Table 2 led to similar findings and conclusions. The corresponding reduction factors are presented in Table 9 and illustrated in Figure 20. Most of the simulated force-displacement curves followed the shape of Figures 1 and 2b for joints typically having large and small β values, respectively. The results also show that parameter β affects the joint resistance and must be considered in the joint design.

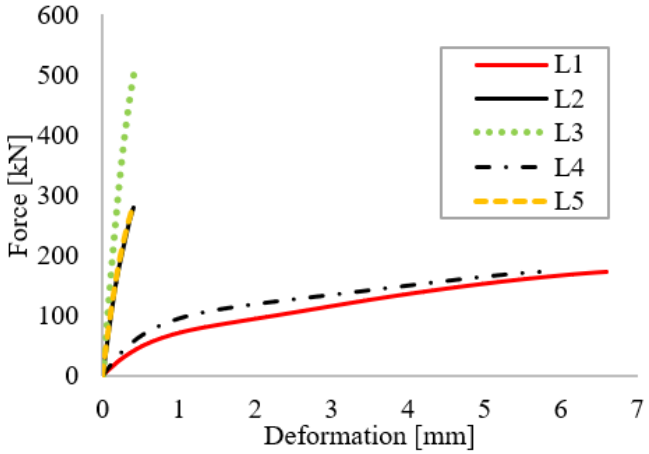

Fig. 18: Force-displacement curves of numerical models at 500 ℃. The 1%b_0- and 3%b_0-limit values correspond to 2 mm and 6 mm displacements.

Tab. 8. Reduction in axial resistance of SHS T-joints at elevated temperatures based on numerical simulations. Ratio of numerical simulation result at temperature θ to Eurocode resistance at 20 ℃.

Models	100	200	300	400	500	600	700	800

	[°C]	[°C]	[°C]	[°C]	[°C]	[°C]	[°C]	[°C]
$k_{y,\theta}$	1.00	1.00	1.00	1.00	0.78	0.47	0.23	0.11
$k_{E,\theta}$	1.00	0.90	0.80	0.70	0.60	0.31	0.13	0.09
L1	1.00	0.93	0.85	0.73	0.60	0.33	0.15	0.084
L2	1.00	0.92	0.83	0.72	0.59	0.33	0.15	0.088
L3	1.00	0.94	0.79	0.75	0.61	0.34	0.16	0.088
L4	1.00	0.94	0.87	0.77	0.63	0.31	0.16	0.092
L5	1.00	0.92	0.83	0.72	0.59	0.33	0.15	0.088
Average, k_{FEM}	1.000	0.928	0.837	0.739	0.604	0.327	0.153	0.088

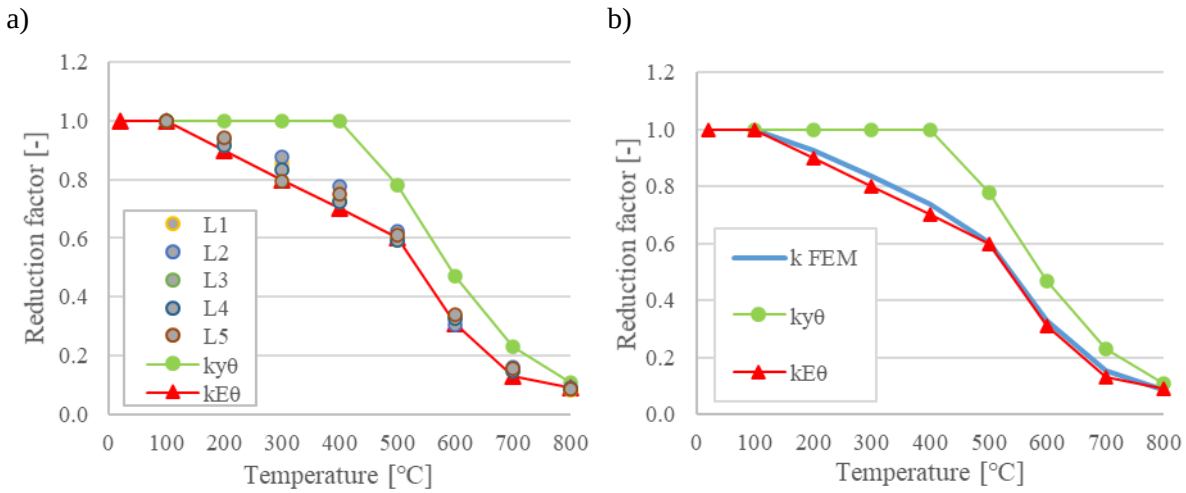

Fig. 19. Relationship between the reduction in joint resistance and joint temperature: a) for specimens L1- L5; b) average value of specimens L1-L5.

Tab. 9. Reduction in axial resistance of SHS T-joints at elevated temperatures based on numerical simulations. Ratio of numerical simulation result at temperature θ to Eurocode resistance at 20 °C.

Models	100 [°C]	200 [°C]	300 [°C]	400 [°C]	500 [°C]	600 [°C]	700 [°C]	800 [°C]
$k_{y,\theta}$	1.00	1.00	1.00	1.00	0.78	0.47	0.23	0.11
$k_{E,\theta}$	1.00	0.90	0.80	0.70	0.60	0.31	0.13	0.09
P1	1.000	0.907	0.813	0.686	0.568	0.313	0.144	0.081
P2	1.000	0.930	0.853	0.729	0.597	0.333	0.155	0.084
P3/10	1.000	0.939	0.875	0.774	0.625	0.307	0.161	0.092
P4	1.000	0.962	0.923	0.784	0.623	0.362	0.172	0.088
P5	1.000	0.969	0.931	0.861	0.738	0.513	0.287	0.156
P6	1.000	0.915	0.831	0.722	0.594	0.328	0.148	0.088
P7	1.000	0.981	0.959	0.888	0.786	0.558	0.334	0.191
P21/8	1.000	0.963	0.924	0.792	0.628	0.367	0.175	0.089
P9	1.000	0.965	0.935	0.796	0.631	0.370	0.176	0.089
P11	1.000	0.933	0.867	0.743	0.600	0.333	0.152	0.086
P19	1.000	0.954	0.905	0.790	0.629	0.365	0.173	0.089
P20	1.000	0.962	0.922	0.794	0.630	0.369	0.175	0.089
P22	1.000	0.961	0.926	0.786	0.625	0.364	0.173	0.090
P23	1.000	0.960	0.918	0.773	0.618	0.357	0.167	0.088
Average, k_{FEM}	1.000	0.950	0.899	0.780	0.635	0.374	0.185	0.100

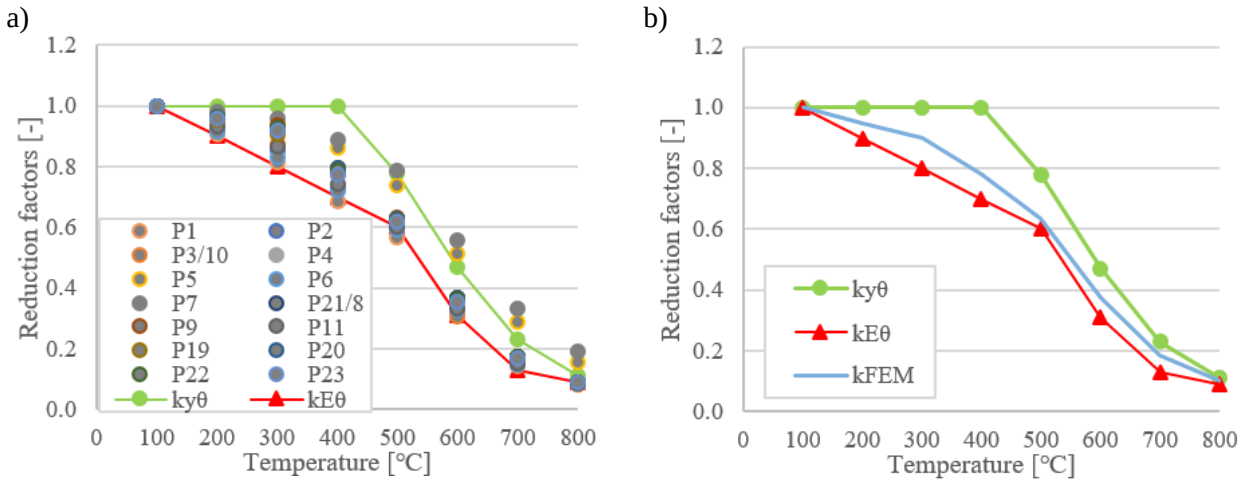

Fig. 20. Relationship between the reduction in joint resistance and joint temperature: a) for simulation models P1-P23; b) average value of specimens P1-P23.

The above simulation results and observations show that using the reduction factor for the elastic modulus of steel leads to a close and conservative lower bound approximation to the joint resistance reduction at elevated temperatures. Based on the experimental test results and the numerical simulations reported, it can be proposed that the axial resistance of welded SHS T-joints in brace compression can be calculated by using the equations of EN 1993-1-8 [1] and modifying the yield strength of steel by the elastic modulus reduction factor. These results are also in line with the numerical findings by Ozyurt et al. [8].

6. Non-uniform temperature distribution

As presented in previous studies, the temperature distribution within SHS joints is non-uniform [16-18]. The magnitude of the temperature difference depends on connection type and geometry. Typically, the temperatures in the vicinity of the joint are lower than the temperatures further away from the join intersection.

In this section, the component method was applied to demonstrate the difference in resistance between values calculated, assuming non-uniform and uniform joint temperatures. The steel temperatures representing the non-uniform distribution were taken from a numerical model developed in Abaqus CAE software. The model was validated and verified in [17] to represent the temperature distribution of SHS joints. For example, temperature distribution of a joint connecting a SHS 100x5 brace member to a SHS 200x5 chord is presented in Figure 21. The joint temperatures representing the uniform case were calculated according to sub-clause 4.2.5.1 of EN 1993-1-2 [9]. Chord temperature was used in the design and the temperature was calculated using a section factor based on the chord geometry.

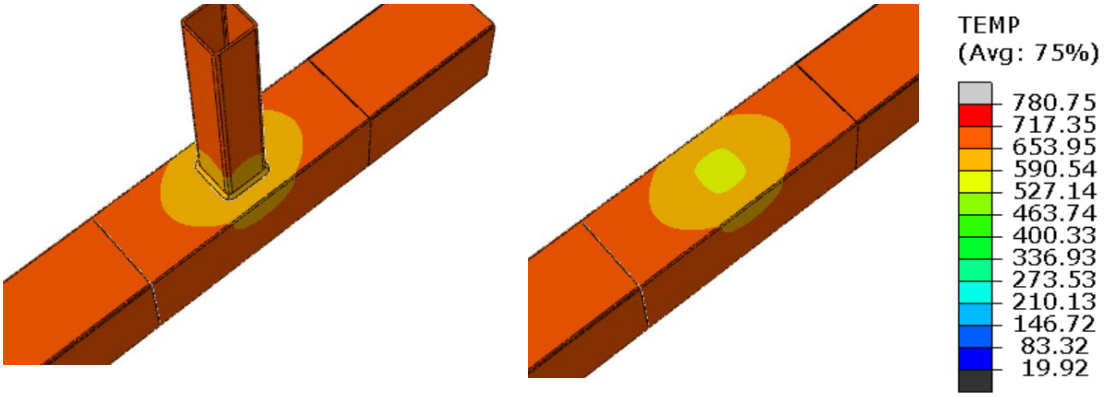

Fig. 21. Numerically determined temperature distribution of a SHS T-joint at 15 min after the commencement of the standard fire exposure.

First, the five specimens used in the experimental tests were analysed (refer to Table 1). Temperatures of the connection components were determined and the corresponding component and joint axial resistances were calculated every five minutes using Equations (2)-(4). For the non-uniform distributions, three different steel temperatures were determined, using the numerical model. Chord face temperature was taken as the average of four points located on all sides of the brace and 5 mm away from the face of the brace. Chord side wall temperature was calculated as the average of two points, located on both sides of the chord at mid-height of the chord side wall and at the brace centreline. Brace temperature was calculated as the average of four points located on all sides of the brace and 5 mm above the chord face. The calculated joint resistance values in brace axial compression at different time steps are reported in Table 10. The weakest connection components revealed in the component method corresponded to experimental and numerical analysis results. For the uniform temperature situation, the joint temperature development was calculated using the equations for unprotected internal steelwork given in EN 1993-1-2 [9]. The calculated joint resistance values are presented in Table 11.

Next, strength of the joints calculated by the component method with non-uniform temperature increase of the joint (N_{NUN}) was then compared with the calculation of the joints' strength, assuming the uniform temperature distribution of the joint (N_{UN}) as proposed in the EN 1993-1-2 [9]. The ratio N_{NUN}/N_{UN} is summarized in Table 12 and illustrated in Figure 22. Table 12 and Figure 22 include results for each specimen and the average value for all specimens. It can be seen that the exact temperature field gives an advantage of higher strength of the joint, especially for joints with a bigger β parameter and a thicker chord wall than brace wall. The general increase of strength, considering the non-uniform temperature, was 20%.

Tab. 10. Strength of the SHS T-joints at elevated temperatures obtained for non-uniform temperature distribution, $N_{1,Rd,fi}$ [kN].

N_{NUN}	Time [min]						
	0	5	10	15	20	25	30
L1	95.17	95.17	62.20	28.38	19.28	16.59	12.52
L2	315.18	306.40	224.93	102.50	61.75	53.85	44.43
L3	899.45	882.58	799.09	430.18	227.07	168.33	149.95
L4	115.90	115.90	77.50	35.29	23.64	20.35	15.66
L5	315.18	306.40	224.93	102.50	61.75	53.85	44.43

Tab. 11. Strength of the SHS T-joints at elevated temperatures obtained for uniform temperature development of EN 1993-1-2, $N_{1,Rd,fi}$ [9].

N_{UN}	0 [min]	5 [min]	10 [min]	15 [min]	20 [min]	25 [min]	30 [min]
L1	95.17	95.17	53.80	24.08	17.79	11.92	8.95
L2	315.18	303.98	169.04	73.60	54.83	37.45	29.12
L3	899.45	878.74	720.31	327.20	172.34	143.46	91.32
L4	115.90	115.90	64.78	28.84	21.64	14.43	10.95
L5	315.18	303.98	169.04	73.60	54.83	37.45	29.12

Tab. 12. Comparison of strength of the SHS T-joints at elevated temperatures obtained with non-uniform and uniform temperature distribution.

N_{NUN}/N_{UN}	0 [min]	5 [min]	10 [min]	15 [min]	20 [min]	25 [min]	30 [min]
L1	1.000	1.000	1.156	1.179	1.084	1.392	1.399
L2	1.000	1.008	1.331	1.393	1.126	1.438	1.526
L3	1.000	1.004	1.109	1.315	1.318	1.173	1.642
L4	1.000	1.000	1.196	1.224	1.092	1.410	1.430
L5	1.000	1.008	1.331	1.393	1.126	1.438	1.526
Average[AV]	1.000	1.004	1.225	1.300	1.149	1.370	1.505

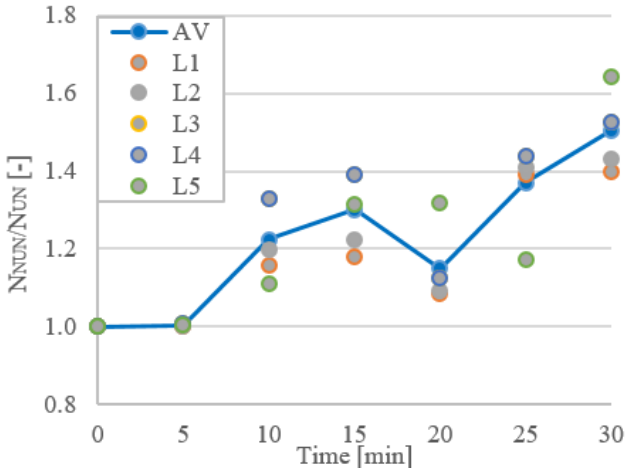

Fig. 22. Comparison of strength of the SHS T-joints at elevated temperatures obtained with non-uniform and uniform temperature distribution.

The same analysis was then performed for the joints of the parametric study. The joint resistance values were calculated with the non-uniform and uniform temperature distributions, as described above. The obtained results of the comparison N_{NUN}/N_{UN} are summarized in Table 13 and Figure 23.

Tab. 13. Comparison of strength of the SHS T-joints at elevated temperatures obtained with non-uniform and uniform temperature distributions.

N_{NUN}/N_{UN}	0 [min]	5 [min]	10 [min]	15 [min]	20 [min]	25 [min]	30 [min]
P1	1.00	1.00	1.13	1.14	1.08	1.40	1.37
P2	1.00	1.00	1.13	1.14	1.08	1.40	1.37
P3/10	1.00	1.00	1.22	1.22	1.09	1.41	1.42
P4	1.00	1.00	1.25	1.28	1.11	1.40	1.49

P5	1.00	1.00	1.33	1.37	1.14	1.44	1.58
P6	1.00	1.01	1.33	1.39	1.13	1.43	1.52
P7	1.00	1.00	1.03	1.31	1.42	1.16	1.49
P21/8	1.00	1.00	1.11	1.25	1.21	1.16	1.65
P9	1.00	1.00	1.17	1.24	1.11	1.30	1.56
P11	1.00	1.00	1.20	1.15	1.09	1.48	1.17
P19	1.00	1.00	1.07	1.15	1.18	1.12	1.63
P20	1.00	1.00	1.08	1.17	1.15	1.14	1.64
P22	1.00	1.00	1.20	1.28	1.13	1.31	1.58
P23	1.00	1.00	1.26	1.30	1.11	1.42	1.47
Average[AV]	1.00	1.00	1.18	1.24	1.14	1.33	1.50

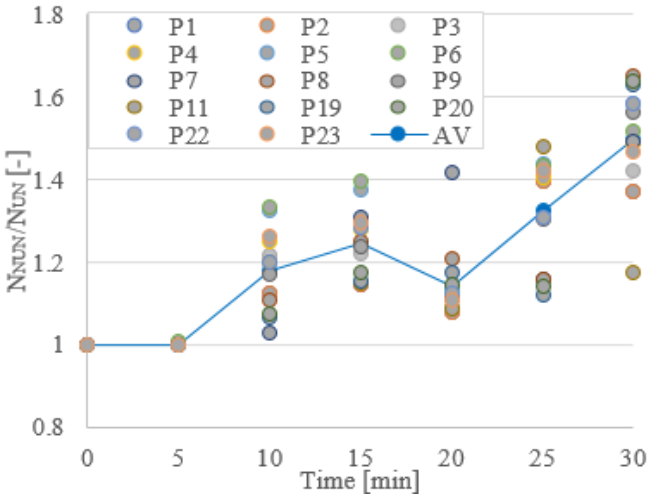

Fig. 23. Comparison of strength of the SHS T-joints at elevated temperatures obtained with non-uniform and uniform temperature distributions.

The aim of the study was to determine whether more detailed joint temperature distribution provides a more reliable and economical design, compared to the use of constant temperature for all connection components. The results presented indicate that, by utilizing more accurate information in joint resistance calculations, on average, 20 % higher resistance values can be obtained, compared to the approach in which uniform temperature distribution is assumed, and the joint temperature is determined using the formulae of EN 1993-1-2 [9]. However, obtaining the exact temperature distribution for every joint is time-consuming and not feasible. Uniform temperature distribution and the Eurocode approach are considered conservative and safe assumptions for the SHS T-joint design. Based on the results presented in Baczkiewicz et. al [17-18] the temperature of a joint intersection can be calculated as the average value of the chord and brace temperatures determined using the formulae of EN 1993-1-2 [9]. This estimation leads to a safe prediction of strength reduction, without overestimating the temperature.

7. Conclusions

This paper presented a numerical study of the performance of SHS T-joints under brace axial compression in fire conditions. Based on the results and observations, the following conclusions can be asserted:

(1) The critical temperature of the joint is mostly influenced by the geometric ratio β and the level of the applied load. The effects of other geometric parameters were found to be insignificant.

(2) The design axial resistance of a welded compressed joint can be calculated using the design equations of EN 1993-1-8 [1], provided that steel strength at elevated temperatures is modified by the reduction factor of steel elastic modulus, in accordance with EN 1993-1-2 [9].

(3) By utilizing more accurate temperature distribution in the joint resistance calculations, on average, 20 % higher resistance values can be obtained, compared to the approach in which uniform temperature distribution is assumed. Obtaining more accurate distribution is, however, very time-consuming and, therefore, not feasible. Based on the results, a conservative estimation of the joint temperature can be provided by using the mean value of chord and brace temperatures calculated based on the equations of EN 1993-1-2 [9].

References

[1] EN 1993-1-8: Eurocode 3: Design of steel structures. Part 1-8: Design of joints, European Committee for Standardization (CEN), Brussels, 2005.

[2] CIDECT. Design guide for circular hollow section (CHS) joints under predominantly static loading, Verlag TUV Rheinland, Germany; 2010.

[3] Liu M., Zhao J., Jin M. An experimental study of the mechanical behaviour of steel planar tubular trusses in a fire. Journal of Constructional Steel Research 66(4), pp. 504-511, 2010.

[4] Jin M., Zhao J., Liu M., Chang J. Parametric analysis of mechanical behaviour of steel planar tubular truss under fire. Journal of Constructional Steel Research 67, pp. 75-83, 2011.

[5] Chen C., Shao Y., Yang J. Experimental and numerical study on fire resistance of circular tubular T-joints. Journal of Constructional Steel Research 85, pp. 24-39, 2013.

[6] Tan K., Fung T., Nguyen M.P. Structural behaviour of CHS T-joints subjected to brace axial compression in fire conditions. Journal of Structural Engineering 139 (1), pp. 73–84, 2013.

[7] He S., Shao Y., Yang D., Long F. Experimental study on circular hollow section (CHS) tubular K-joints at elevated temperature. Engineering Failure Analysis 34, pp. 204-216, 2013.

[8] Ozyurt E., Wang Y.C., Tan K.H. Elevated temperature resistance of welded tubular joints under axial load in the brace member. Engineering Structures 59, pp. 574-586, 2014.

[9] EN 1993-1-2: Eurocode 3: Design of steel structures. Part 1-2: General rules – Structural fire design, European Committee for Standardization (CEN), Brussels, 2005.

[10] Lan, X., Huang, Y. Structural design of cold-formed stainless steel tubular X- and T-joints at elevated temperatures, Thin-Walled Structures, 108, pp. 270 – 279, 2016.

[11] He S., Shao Y., Yang D., Zhang H., Wang Q. Parametric study on performance on circular tubular K-joints at elevated temperature. Fire Safety Journal 71, pp. 174-186, 2015.

[12] Shao Y., Zheng Y., Zhao H., Yang D. Performance of tubular T-joints at elevated temperature by considering effect of chord compressive stress. Thin-walled Structures 98, pp. 533-546, 2016.

[13] American Petroleum Institute (API), Recommended Practice for Planning, Designing and Constructing Fixed Offshore Platforms—Working Stress Design, 21st Ed., API Recommended Practice 2A WSD (RP 2A WSD), Washington, DC, 2000.

[14] Shao Y., He S., Yang D. Prediction of static strength for CHS tubular K-joints at elevated temperature. Journal of Civil Engineering 21(3), pp. 900-911, 2017.

[15] Yang J., Shao Y., Chen C. Experimental study on fire resistance of square hollow section (SHS) tubular T-joint under axial compression. Advanced Steel Construction 10, pp. 72-84, 2014.

[16] Bączkiewicz J., Malaska M., Pajunen S., Heinisuo M., Experimental study on axially loaded square hollow section T-joints under fire conditions. Fire Safety Journal 114, 102993, 2020.

[17] Bączkiewicz J., Malaska M., Pajunen S., Heinisuo M., Experimental and numerical study on temperature distribution of welded square hollow section joints. Journal of Constructional Steel Research 142, pp. 31-43, 2018.

[18] Bączkiewicz J., Malaska M., Pajunen S., Heinisuo M., Parametric study on temperature distribution of square hollow section joints. Journal of Constructional Steel Research 160, pp. 490-498, 2019.

[19] Zhao X.-L. Deformation limit and ultimate strength of welded T-joints in cold-formed RHS sections. Journal of Constructional Steel Research 53(2), pp. 149–165. 2000

[20] Lu L.H., de Winkel G.D., Yu Y. & Wardenier J. 1994. Deformation limit for the ultimate strength of hollow section joints. In P. Grundy, A. Holgate, & B. Wong, eds. Tubular Structures VI, 6th International Symposium on Tubular Structures, Melbourne, Australia. Rotterdam: Balkema, pp. 341–347.

[21] EN 1993-1-1: Eurocode 3: Design of steel structures. Part 1-1: General rules and rules for buildings, European Committee for Standardization (CEN), Brussels, 2005.

[22] Jaspart J.-P., Pietrapertosa C., Weynand K., Busse E. & Klinkhammer R. Development of a full consistent design approach for bolted and welded joints in building frames and trusses between steel members made of hollow and / or open sections – Application of the component method. Volume 1 – Practical guidelines, CIDECT Report: 5BP-4/05, 2015.

[23] Weynand K., Jaspart J.-P., Demonceau J.F. & Zhang, L. Component method for tubular joints, CIDECT Report 16F – 3/15, 2015.

[24] CEN/TS 1993-1-801, Eurocode 3 - Design of steel structures - Part 1-801 Hollow section joint design according to the component method. Accepted.

[25] Jaspart JP., Weynand K., Demonceau JF., CEN technical specification for design of hollow section joints according to the component method. *Proceedings* of the 17th International Symposium on Tubular Structures, Singapore, pp. 543-549, 2019.

[26] Wardenier J. Hollow section joints, Delft University Press, 1982.

[27] Garifullin M. Component Method for High Strength Steel Rectangular Hollow Section T Joints. (Tampere University Dissertations; Vol. 45). Tampere University, 2019.

[28] ABAQUS CAE 2017 User's Manual Dassault Systems, 2017.

Declaration of interests

☒ The authors declare that they have no known competing financial interests or personal relationships that could have appeared to influence the work reported in this paper.

☐The authors declare the following financial interests/personal relationships which may be considered as potential competing interests:

Jolanta Bączkiewicz: Data curation Software, Writing- Original draft preparation.: **Mikko Malaska**: Methodology, Writing- Reviewing and Editing.: **Sami Pajunen**: Conceptualization, Writing- Reviewing and Editing.: **Markku Heinisuo**: Supervision: